Nature of the crust beneath the islands of the Mozambique Channel: Constraints from receiver functions

Anthony Dofal, Fabrice R. R Fontaine, Laurent Michon, Guilhem Barruol, Hrvoje Tkalčić

Nature of the crust beneath the islands of the Mozambique Channel: Constraints from receiver functions

A. Dofal [a,b,*], F.R. Fontaine [a,b,c], L. Michon [a,b], G. Barruol [a], H. Tkalčić [d]

[a] *Université de Paris, Institut de Physique Du Globe de Paris, CNRS, F-75005, Paris, France*
[b] *Université de La Réunion, Laboratoire GéoSciences Réunion, F-97744, Saint Denis, France*

[c] *Observatoire Volcanologique et Sismologique de La Martinique, Institut de Physique Du Globe de Paris, F-97250, Fonds Saint Denis, France*
[d] *Research School of Earth Sciences, The Australian National University, Canberra, ACT, 2601, Australia*

ABSTRACT

Starting in May 2018, a volcano-tectonic crisis occurred in the vicinity of Mayotte, a volcanic island in the Comoros Archipelago in the Mozambique Channel. The origin of the volcanism but also the subsurface archi-tecture and nature of the crust, remain unknown. Here, based on receiver function analyses that provide *S*-wave velocity profiles, we determine the depth of Mohorovičić discontinuity (*Moho*) and Vp/Vs ratios for volcanic islands in the Mozambique Channel. We propose that the crust beneath Mayotte and Juan de Nova islands is of continental nature, while it appears to be of oceanic origin beneath Europa and Grande Glorieuse islands. Our results suggest that Mayotte edifice grew on an isolated continental block abandoned during the Gondwana breakup and the opening of the Mozambique Channel. The continental crust is underlain by a thick (9–10 km) and fast layer, interpreted as magmatic underplating which may result from the 20-Myr-long duration of the volcanism. The new velocity model determined from the seismic station on Mayotte can be used to relocate the seismicity related to the ongoing volcano-tectonic crisis.

1. Introduction

In the Mozambique Channel, the nature of the lithosphere and the location and geometry (sharp or broad) of the Ocean-Continent transition are still under debate (Fig. 1A). In the Mozambique Basin, i.e. in the southern part of the Mozambique Channel, successive campaigns involving magnetic, seismic reflection and refraction surveys led to a consensus about the oceanization processes and the oceanic nature of the crust (e.g. Leinweber and Jokat, 2012; Senkans et al., 2019). In the northern Mozambique Channel, i.e. the southern Somali Basin and the Comoros Basin, two hypotheses regarding the nature of the crust have been proposed. Talwani (1962) suggested from isostatic data an abnormal oceanic crust, while slight magnetic anomalies in the Comoros Basin led Lort et al. (1979) to propose a continental crust in the southern half of the northern Mozambique Channel. Recent geophysical data confirm a continental nature of the crust limited to the western and southern parts of the Comoros Basin (Klimke et al., 2016; Roach et al., 2017; Vormann et al., 2020) and an oceanic crust beneath its northern half (Vormann et al., 2020). However, the occurrence of quartzite inclusions in volcanic rocks from the Comoros Archipelago, limiting the Comoros Basin in the north (Flower and Strong, 1969), and the presence of a massif of quartzite on the island of Anjouan (Fig. 1B; Flower, 1972) suggest that this archipelago could be built on a continental crust or at least over continental crust slices. Thus, the location of the Ocean-Continent transition in the northern Mozambique Channel remains unclear.

In May 2018, a seismic crisis associated with the appearance and building of a new submarine volcano started east of Mayotte Island (see the seismic swarm in Fig. 1B; Bulletins from the volcanological and seismological monitoring network of Mayotte: ReVoSiMa, http://www.ipgp.fr/revosima; Cesca et al., 2020; Lemoine et al., 2020; Feuillet et al., 2021). The new volcano represents a new threat for the population of surrounding islands. Thus, in order to improve our knowledge on the nature of the crust in the Mozambique Channel and to better relocate the volcano-tectonic seismicity close to Mayotte, we investigate the crustal structure beneath seismic stations deployed on several volcanic edifices of the region (Mayotte, Grande Glorieuse, Juan de Nova and Europa; Fig. 1) and along the southeastern part of Madagascar, chosen as a "continental" reference. We applied the receiver function (RF) technique on the seismic records from land seismic stations deployed temporarily

* Corresponding author. Université de Paris, Institut de physique du globe de Paris, CNRS, F-75005, Paris, France.
E-mail address: anthony.dofal@univ-reunion.fr (A. Dofal).

during the RHUM-RUM experiment (Réunion Hotspot and Upper Mantle – Réunion Unterer Mantel, Barruol and Sigloch, 2017, Barruol and Sigloch, 2013 www.rhum-rum.net). This limited RFs dataset has been inverted with the Neighborhood Algorithm (NA, Sambridge, 1999) to determine the *S*-wave velocity structure beneath all stations. Furthermore, we used the *H*-κ stacking method (Zhu and Kanamori, 2000) to constrain the mean crustal V_P/V_S ratio and the mean *Moho*-depth values and consequently increase the robustness of our interpretations.

2. Geological context

The Mozambique Channel results from the dismantling of the Gondwana along the East African margin, which started with a Permo-Triassic rifting phase (e.g. Cox, 1992). The syn-rift sediment sequence called Karoo is found in basins such as the Morondava and Majunga Basins (e.g. Rogers et al., 2000), along the Davie Ridge (Bassias and Leclaire, 1990) and the central Mozambique margin (Senkans et al., 2019). From the Middle Jurassic to the Early Cretaceous, the Davie Ridge accommodated the opening of two basins (Coffin and Rabinowitz, 1987). In the north, the Somali Basin resulted from the southward drift of Madagascar leading to oceanic accretion between ~150 and 120 Ma (Ségoufin and Patriat, 1981) with N–S crustal extension along E-W trending ridges (Davis et al., 2016) supported by magnetic anomalies (Phethean et al., 2016) and *SKS* splitting measurements (Scholz et al., 2018) compatible with ridge-parallel asthenospheric flow. In the south, the Mozambique Basin is due to the separation of Africa and Antarctica that started at the end of the Jurassic (Konig and Jokat, 2010; Leinweber et al., 2013) and finished during the Early Cretaceous (e.g. Rabinowitz et al., 1983).

An intense volcanic phase related to the Marion hotspot activity took place during the Upper Cretaceous (Chatterjee et al., 2013). It likely participated in the separation of India from Madagascar (Storey et al., 1995), the building of submarine magmatic plateaus (e.g. Madagascar Rise; Zhang et al., 2011), and flood basalts covering parts of Madagascar (de Wit, 2003). Grande Glorieuse Island, associated to the NW-SE volcanic alignment of Aldabra, may be linked to this activity (Courgeon et al., 2016).

The last volcanic episode in the Mozambique Channel seems to be related to the activity of the Tertiary East African Rift System (EARS; Fig. 1B; Michon, 2016; Famin et al., 2020). The volcanism of several islands (Comoros Archipelago, Bassas da India) and seamounts (Sakalaves along the Davie Ridge and Natal seamounts) is coeval with the volcanism of the EARS (e.g. Courgeon et al., 2016, 2018; O'Connor et al., 2019). Moreover, the location of the seismicity along the Comoros Archipelago, the Davie Ridge and the Quathlamba Seismic Axis favors a southward continuity of the EARS in the Mozambique Channel (Hartnady, 1990). Tectonic deformation revealed by seismic reflection studies supports this hypothesis (Franke et al., 2015; Deville et al., 2018).

At upper mantle scale, structures display strong latitudinal variations along the Mozambique Channel that may explain the past and recent volcano-tectonic activity. Surface wave tomographies (Mazzullo et al., 2017) evidence thick and fast lithosphere (more than 100 km) in the central part of the Mozambique Channel, thinning further south in the Mozambique Basin and also thinning to the north beneath the Comoros Archipelago and the Somali Basin. Mayotte hence appear to be sitting above a thinner lithosphere (~80 km) overlying a hotter than normal asthenosphere spreading from the Mascarene Basin further east (Barruol et al., 2019).

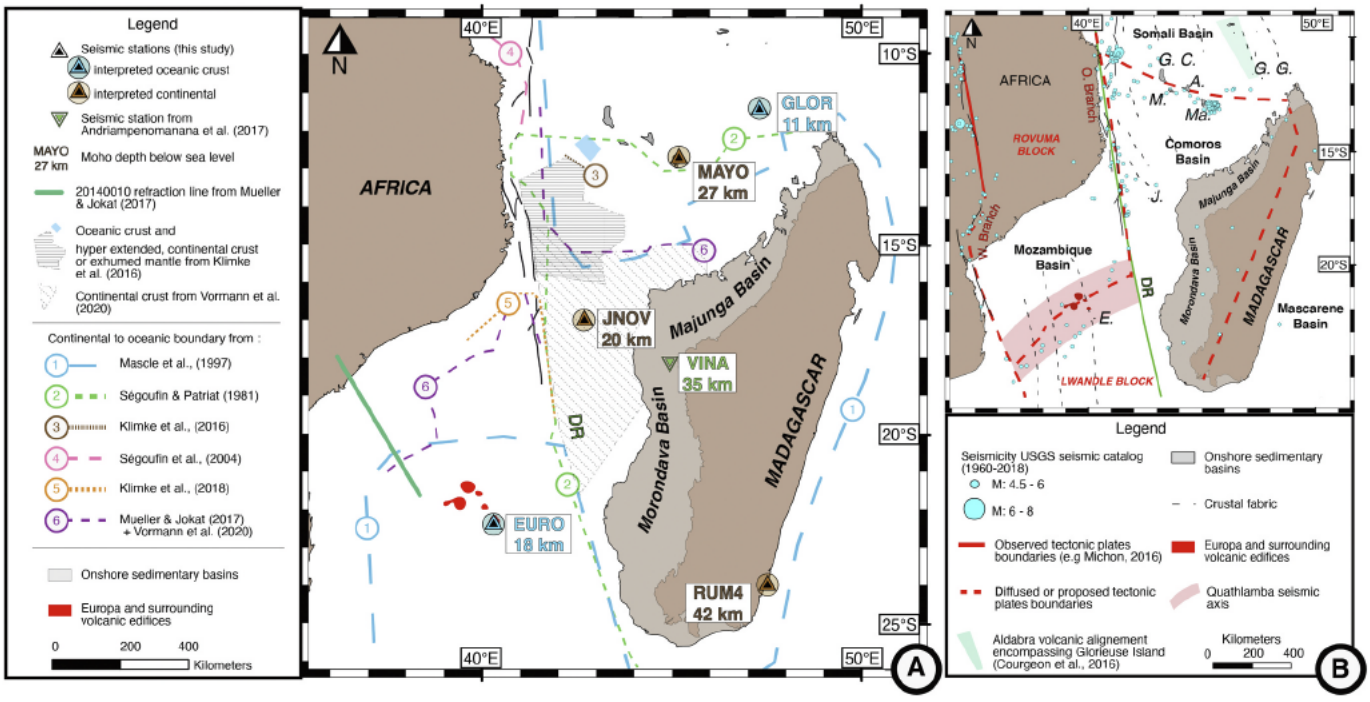

Fig. 1. General map of the studied area. (A): Location of the seismic stations used in this study (triangles). Seismic station GLOR, MAYO, JNOV, EURO and RUM4 stands for Grande Glorieuse Island, Mayotte Island, Juan de Nova Island, Europa Island and a station located on the eastern coast of Madagascar, respectively. VINA is a station from the study of Andriampenomanana et al. (2017), which revealed a crustal thickness of 35 km. Color lines and the referred number accounts for several proposed Continental-Ocean Boundary (COB) or Ocean-Continent transition (OCT): (1) Mascle et al., 1987; (2) Ségoufin and Patriat (1981); (3) Klimke et al. (2016); (4) Ségoufin et al. (2004); (5) Klimke et al. (2018); (6) Mueller and Jokat (2017). (B) Structural map of the Mozambique Channel. Red lines indicate tectonic plate boundaries while dashed red lines indicates diffuse or proposed tectonic boundaries (e.g. Stamps et al., 2008; Famin et al., 2020). Blue dots: location of the seismicity provided by the USGS between 1960 and 2018. Red area represents the Quathlamba Seismic Axis and green area stands for the volcanic edifice alignment of Grande Glorieuse (Courgeon et al., 2017). G. C. stand for Grande Comore; A. Anjouan; M., Mohéli; Ma., Mayotte; G. G., Grande Glorieuse; J., Juan de Nova Island and E., Europa Island. Finally, DR stands for Davie Ridge. (For interpretation of the references to color in this figure legend, the reader is referred to the Web version of this article.)

3. Data and methods

We retrieved seismic waveforms from 5 broad-band seismic stations from the RHUM-RUM experiment (Barruol et al., 2017; https://doi.org/10.15778/RESIF.YV2011) located on Mayotte (MAYO), Grande Glorieuse (GLOR), Juan de Nova (JNOV) and Europa (EURO) islands and finally the eastern coast of Madagascar (RUM4; Fig. 1A). Full details of data are available in Table S1.

We used two *P*-wave RFs methods (see details in the supplementary material: Text S1) to characterize the crustal structure and the *Moho* depth below each station, as previously described in several studies (Fig. S2; e.g. Fontaine et al., 2013a,b; 2015; Lamarque et al., 2015). Seismic records from teleseismic events were selected by (1) an epicentral distance located between 25° and 90° from the station (Fig. S1), (2) a magnitude higher than 5.5 and (3) a Signal-to-Noise Ratio (SNR) larger than 2. The data were cut 5 s prior and 30 s after the *P*-wave before the iterative time domain deconvolution to compute *P*-wave RFs (Ligorria and Ammon, 1999).

The Neighborhood Algorithm (NA) inversion method (Sambridge, 1999) was applied to compute an ensemble of solutions of *S*-wave velocities (V_S) profiles (Fig. 2; see details in the supplementary material: Text S1). Radial RFs were grouped by back-azimuths and by ray parameters satisfying $p_{median} \pm 0.006$ s km^{-1} to compute the average RF in each 90° quadrant in order to minimize the possible effects of crustal anisotropy and dipping seismic interfaces (see Fontaine et al., 2013a for further details). The quadrant presenting the maximum numbers of constraints, (i.e with the highest number of RFs) has been used for the stacking procedure. To determine the velocity interfaces from the *S*-wave velocity (V_S) profiles, we considered the 1000 best fitting models and their average (black line in Fig. 2F-J).

We also applied the *H*-κ stacking method on the dataset to determine which interface modeled by the NA corresponds to the *Moho* (Zhu and Kanamori, 2000; see details in the supplementary material: Text S1). For the *H*-κ stacking method, the whole set of RFs is used without distinction of back-azimuth. By determining the time lag between the *P* and the P_{ms} phase and between the P_{ms} phase and its crustal multiples (*PpPms* and *PpSms* + *PsPms*) and assuming a constant crustal velocity, this method allows to jointly determine the *Moho* depth (*H*) and the V_P/V_S ratio (κ), this latter being a good proxy of the crustal nature. The definition of each phase is fully detailed in Fig. S3. Results are presented in Fig. 3.

4. Results

Madagascar. Seismic records from RUM4 station display the highest SNR of the study (Fig. S2A). The ensemble of RFs (i.e., 5 RFs) and the stacked RF obtained for the NA show the P_{ms} phase at ~5 s after the direct *P* phase (Fig. 2A). The modeled RF describing the average of the 1000 best velocity models in Fig. 2A shows an excellent fit with the data. The *S*-wave velocity curve obtained from the NA inversion presents a constant velocity gradient down to around 32 km, then an increase of the velocity until *Vs* 4.4 km/s at 42 km depth (Fig. 2F). The *H*-κ stacking results confirm that the *Moho* likely lies at 42 km depth and indicate an average V_P/V_S ratio below the station of 1.68 ± 0.05 (Fig. 3A).

Europa Island. Seismic records from EURO station display a smaller SNR than at the other stations, which probably explains the lower quantity of RFs (i.e. 4 RFs; Table S3; Fig. S2B). The stacked RF (Fig. 2B) shows a P_{ms} phase at almost 1.3 s after the direct *P* phase, similarly than

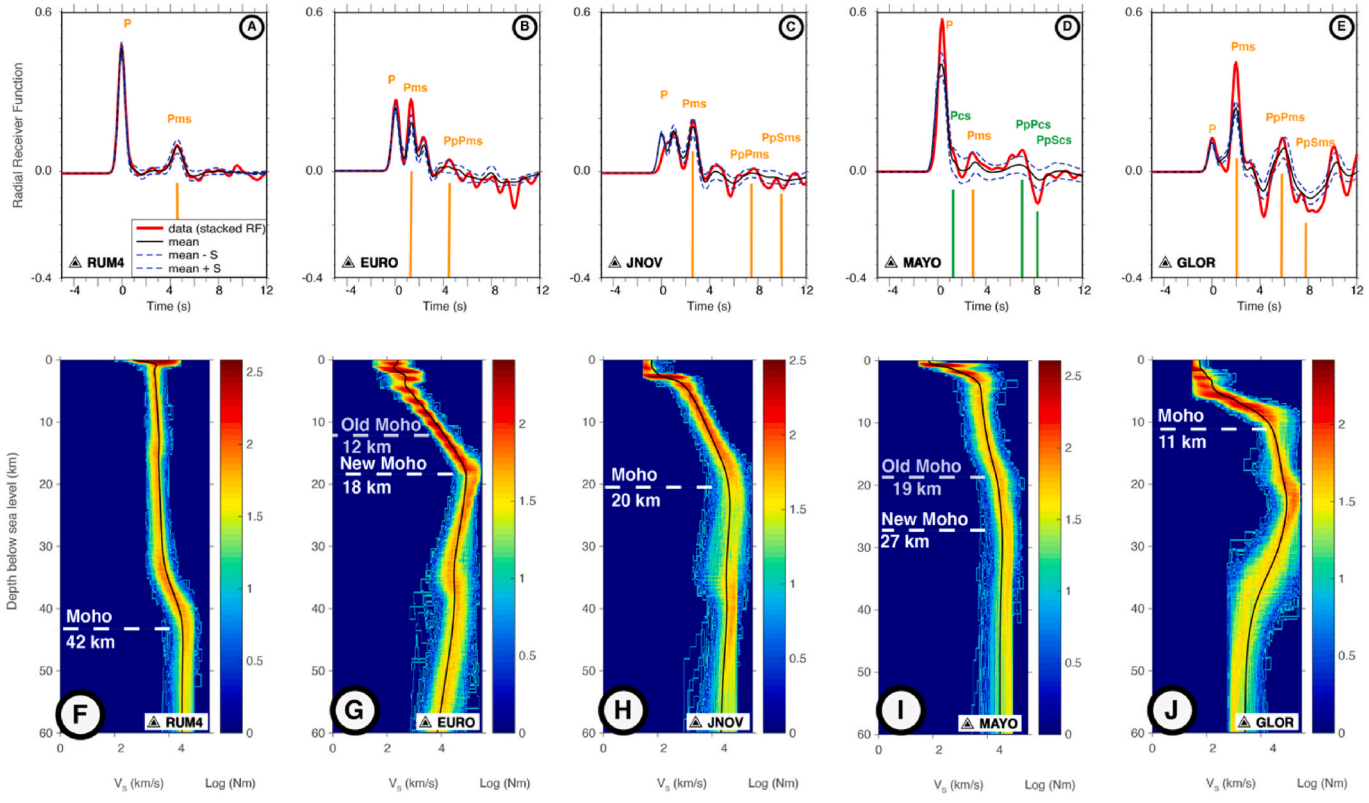

Fig. 2. Receiver function analyses: results of the NA inversion at the five studied seismic stations RUM4, EURO, JNOV, MAYO and GLOR. A–E: comparison between the measured RF in red and the mean RF determined from the best 1000 models resulting from the inversion in black with the ±1 standard deviation limits around the average in blue. Orange vertical lines indicate for comparison predicted arrival times of the P_{ms} phase and crustal multiples for the best model resulting from the H-κ stacking model. For MAYO, green vertical lines indicate the Pcs phase (i.e. the phase related to the boundary between the initial crust and the magmatic underplating body) and the multiples. F–J: Density plot of the best 1000 velocity-depth models over the 45 200 models calculated at each site. The color scale is logarithmically proportional to the number of models (Nm). The black line shows the average of the 1000 best models. (For interpretation of the references to color in this figure legend, the reader is referred to the Web version of this article.)

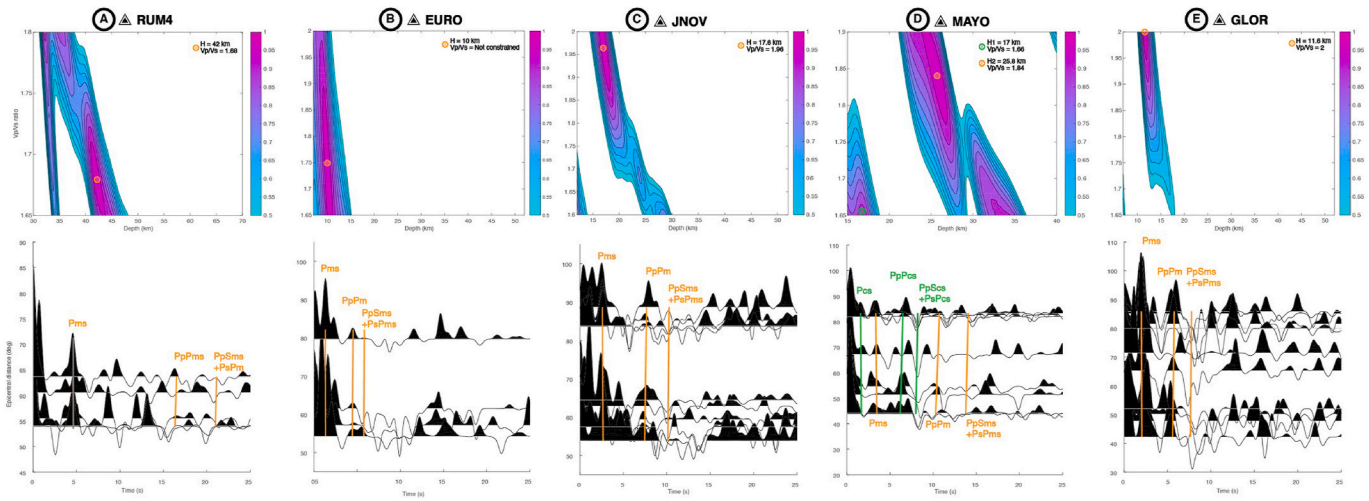

Fig. 3. Upper row: plots of H and κ parameters obtained from the H-κ stacking for RUM4, EURO, JNOV, MAYO and GLOR. The color scale indicates the normalized amplitude of the stack over all back-azimuths along the travel time curves corresponding to the P_{ms} phase and crustal multiples. Lower row: radial receiver functions for these five seismic stations sorted on their increasing epicentral distance. Vertical orange lines indicate predicted arrival times of the P_{ms} phase and crustal multiples for the best model resulting from the H-κ stacking model for a weighting of w_1, w_2 and w_3 of 0.5, 0.5 and 0 respectively. For MAYO station, a specific weighting of $w_1 = 0.7$, $w_2 = 0.3$ and $w_3 = 0$ was applied. Two solutions were obtained for this station and noted H_1 and H_2, with the respective couples of parameters ($H = 17.2$ km; $\kappa = 1.66$) and ($H = 25.8$ km; $\kappa = 1.84$). Predicted arrival times of phases from the H_1 and H_2 solutions are represented correspondingly with green and orange lines. Name of phases for MAYO station are discussed in the text. (For interpretation of the references to color in this figure legend, the reader is referred to the Web version of this article.)

on the whole set of RFs of the station. The average S-wave velocity profile suggests a velocity jump at around 2.5 km depth. From this boundary, a constant velocity gradient is observed down to ~18 km depth. The H-κ stacking method suggests a *Moho* at 10 ± 0.2 km depth. The V_P/V_S ratio is however poorly constrained since the range of ratio with a probability of 0.95 is very wide (Fig. 3B).

Juan de Nova Island. The stacked radial RF determined at JNOV station from NA selected RFs (i.e. 3 RFs) shows similar phases to the individual RFs determined at this station (i.e. 10 RFs; Fig. 2C). Most of these RFs present a clear phase around ~2.7 s after the direct P wave (Fig. 2C). The modeled radial RF obtained with the NA displays two distinct phases between 0 and 1 s, which are shouldered on the average RF, explaining better the first peak (P phase) on the modeled RFs than the average stacked RF. Amplitudes and arrival time of each phase of the modeled RF match the data well. The ensemble of best data-fitting S-wave velocity profiles reveals a seismic discontinuity at depth of ~2.5 km. Another velocity contrast is found at ~20 km below the station (Fig. 2H), and the H-κ stacking suggests a *Moho* depth of 17.6 ± 0.3 km and a high V_P/V_S ratio of 1.96 ± 0.02 (Fig. 3C).

Mayotte Island. The NA stacked radial RF obtained for station MAYO shows a good consistency with all the individual RFs obtained at this station (i.e. 9 RFs; Figs. 2D and S2D). Every RF presents peaks around ~1.2 s, ~3 s, ~6 s and a trough at ~8 s after the direct P wave (Fig. S2D). Results from the H-κ stacking show that the peaks at ~1.2 s and ~3 s could correspond to two *Pms* solutions: H_1 17 ± 3.3 km and a related V_P/V_S 1.66 ± 0 km, and H_2 25.86 ± 3.9 km and V_P/V_S 1.84 ± 0.06, respectively. Arrival times of crustal multiples from H_1 and H_2 solutions are presented in Fig. 3D. The stacked RF is well fitted by the modeled RF explaining the average velocity model of the 1000 best models determined from the NA (Fig. 2D). The predicted RF shows the ~1.2 s that could be convoluted on some RFs and the peak at 3 s (Fig. 2D). The ensemble of best data-fitting S-wave profiles obtained from the inversion of the RF shows a sharp velocity hinge at 4 km beneath the station (Fig. 2I). Beneath this boundary, the S-wave velocity presents a constant velocity gradient down to 19 km depth. Another boundary is also modeled at 27 km depth. These interfaces fit well with the results of the H-κ stacking (i.e., 17 and 26 km; Fig. 3D).

Grande Glorieuse Island. The NA stacked RF calculated for GLOR agrees with the 10 RFs determined at this station (Figs. 2E and S2E). A prominent high amplitude phase arrives 2 s after the P phase on the data and on every RF of this station. It corresponds to the P-wave conversion phase at the *Moho* discontinuity according to H-κ stacking results (P_{ms}; Fig. 3E). Both the arrival times of the P_{ms} phase and crustal multiples for the best model resulting from the H-κ stacking model and amplitudes of theses phases provide a good fit between the modeled RF and the stacked RF (Fig. 2E). The best ensemble of S-wave velocity profiles obtained from the NA inversion shows discontinuities at ~1 and ~5 km depth. At 11 km depth, the NA results suggest a velocity discontinuity that fits well with the determined H-κ stacking *Moho* depth of 11.6 ± 0.02 km (Figs. 2J and 3E). A high V_P/V_S ratio of 2.00 ± 0.02 was obtained beneath GLOR station (Fig. 3E).

5. Discussion

5.1. Structure and nature of the crust in the Mozambique channel

The study of the lithosphere structure from seismometers located on the top of volcanic islands, implies that different kinds of structures may be encountered by seismic waves rising from the deep Earth: the volcanic edifice itself, the sedimentary cover, the underlying crust and the magmatic underplating at the base of the crust. In the following, the structure beneath the station is considered as simple 1-D layered model. To determine the nature of the layers, we compare the average V_P/V_S ratio determined at each station to typical V_P/V_S ratio of felsic and mafic rocks (respectively, <1.78 and >1.81, Artemieva, 2011). The contributions of the sedimentary cover (e.g., Shibutani et al., 1996) with high V_P/V_S ratio, thermal anomalies induced by partial melting or melt occurrence that may increase the V_P/V_S ratio (e.g., Hammond and Humphreys, 2000; Raharjo et al., 2016), and the presence of fluids and extensive silica enrichment that may decrease the V_P/V_S ratio (Zheng and Lay, 2006) were taken into account in the global characterization of the crustal nature. Moreover, we compared our interpretation to regional studies providing information on the sedimentary cover, the possible crustal nature and the available surrounding bathymetry of islands. In the context of volcano-magmatic activity, the structure of the upper lithospheric mantle can be modified as well. Indeed, the

formation of magmatic underplating can change the seismic properties on both sides of the Moho by generating a gradual transition between the crust and the mantle (e.g. Clitheroe et al., 2000). In this case, the highest expected velocity contrast is at the top of the magmatic underplating. In case of underplated magmatic material, a new Moho is determined at the base of a broad transition between crust and mantle (e.g. Fontaine et al., 2013a).

The Madagascar seismic station (RUM4) is used to validate the process by comparing our results with those from Rindraharisaona et al. (2017).

The RUM4 station located in the coastal area of southeastern Madagascar is considered as a typical continental reference. The crust is ~42 km thick and the 1.68 V_P/V_S ratio is in the typical range of continental crust of the Anosyen domain, a continental crust intruded by a magmatic suite between ~550 and 510 Ma (e.g., Tucker et al., 2014). Our results agree well with the previous study of Rindraharisaona et al. (2017), who determined, from the same seismic station but different approaches (joint inversion of RF and surface wave dispersion data and H-κ stacking methods), a *Moho* depth of 38 km and a V_P/V_S ratio of 1.69 (Fig. 3A).

Europa Island. The island stands on a seafloor located at 3 km depth (Smith and Sandwell, 1997). We thus interpret the shallow boundary at 2.5 km depth beneath the seismic station as the limit between the volcanic edifice and the underlying geological formations. This interpretation is supported by the absence of lithosphere flexure beneath Europa Island according to the L7 seismic reflection line of Deville et al. (2018), acquired in the vicinity of the island. Another boundary is observed at 5 km depth in the best ensemble of *S*-wave velocity profiles, which may correspond to the pre-volcanic sediment-to-crust boundary and therefore to a 2.5 km-thick sedimentary layer. This thickness is close to the value (reported as 3.5 km) determined north of the island along the 20140010 refraction line from Mueller and Jokat (2017; Fig. 1A). The discontinuity suggested by the H-κ stacking method at 10 km depth is not marked by a velocity jump on the set of the 1000 velocity curves obtained by the NA. However, assuming an oceanic crustal thickness of 5–7 km, as determined along the 20140010 refraction line (Mueller and Jokat, 2017), the solution proposed by the H-κ stacking (10 km) could correspond to the *Moho* boundary (called the *Old Moho*, Fig. 2G), consistent with a crustal thickness close to the 7 km average thickness of normal oceanic crust (White et al., 1992). The oceanic crustal nature beneath Europa is also supported by magnetic anomalies recorded in the crust (Konig and Jokat, 2010). Another boundary is found at 18 km depth, which we call the *New Moho* (Fig. 2G). Despite a lack of velocity contrast at around 10 km depth in the S-wave velocity profile computed from the NA inversion, we propose that a 6 to 8 km-thick magmatic underplating developed below the volcanic edifice. Such underplating, frequent beneath volcanic islands (e.g. La Réunion, Gallart et al., 1999, Fontaine et al., 2015; Hawaii, Leahy et al., 2010), would have seismic velocities close to that of the upper mantle (Gallart et al., 1999). The occurrence of a relatively thick oceanic crust around Europa is supported by the refraction line AWI-20140010 of Mueller and Jokat (2017), which reveals a crustal thickening towards Europa. Given the location of the island and the magmatic events that occurred in the area (the Marion hotspot and the magmatism related to the EARS; Georgen et al., 2001; Courgeon et al., 2017), such a thick underplating may result from the combined effect of a poly-phase volcanism that started about 90 Ma.

Juan de Nova Island. The island is located between the Davie Ridge and Madagascar on a 2 km deep seafloor (Smith and Sandwell, 1997). The volcanic edifice-to-sedimentary cover boundary is visible on the *S*-wave curve at 2.5 km. Geophysical data suggest that the surrounding basin is underlain by a thinned continental crust (Fig. 1A; Franke et al., 2015; Klimke et al., 2018; Vormann et al., 2020). Moreover, dredged samples on the ridge already suggested a continental nature of the crust (Bassias and Leclaire, 1990). The NA (this study) and Vormann et al. (2020) find a similar *Moho* depth (20 km). Same authors proposed that the sedimentary cover is 4 km thick while the frontier between the sedimentary cover and the crust is not noticeable on the *S*-wave velocity profiles. However, the high V_P/V_S ratio (1.96) is consistent with the occurrence of such sedimentary cover overlying a continental crust and the contribution of thermal anomalies related to the thinning of the crust toward the Davie Ridge is not excluded. Thus, taking into account the thickness of the volcanic edifice (2.5 km) and the sedimentary cover (4 km, from Vormann et al., 2020), the crustal thickness obtained beneath Juan de Nova is 13.5 km, which is consistent with the 12–20 km crustal thinning of a 35 km thick continental crust related to the opening of the Mozambique Channel (Andriampenomanana et al., 2017).

Mayotte Island. The *S*-wave velocity curves determined for Mayotte Island (Fig. 2I) reveal a shallow discontinuity at 4 km depth. The island lies on a 3.5-km-deep surrounding seafloor (Audru et al., 2006) and free-air gravity data beneath the island (Bonvalot et al., 2012) do not show any significant flexure or uplift. Therefore, the shallow discontinuity at 4 km depth is interpreted as the base of the edifice. Further down, our results suggest an interface at 17 km depth and a related V_P/V_S ratio of 1.66 for the lithospheric column between this interface and the station. Our estimate of the V_P/V_S ratio (1.66) is in agreement with that determined from the Wadati method (1933) by the oceanographic MayObs Team surveying the new submarine volcano close to Mayotte coast (Saurel et al., 2019; Saurel et al., under review) and is significantly lower than that of the oceanic crust. Instead, it is in the range of felsic rocks constituting the continental crust (Christensen, 1996; Zheng and Lay, 2006). We consequently interpret this low V_P/V_S ratio as the evidence of a thinned continental crust below Mayotte and the adjacent Anjouan Island where a voluminous massif of quartzite crops out. Another boundary is found at 26–27 km depth with a related average V_P/V_S ratio of 1.84 from this interface to the station. Thus, the layer between these two boundaries (H_1 to H_2) may be described by a high V_P/V_S ratio of 2.16. Such high value of V_P/V_S may indicate the occurrence of mafic to ultra-mafic rocks (Christensen, 1996). Thermal anomaly associated with partial melting may also explain a high ratio (e.g. Hammond and Humphreys, 2000). Therefore, we interpret the H_1 boundary as the *Old Moho* delimiting the thinned continental crust to the magmatic underplating and H_2 as the *New Moho* located between the magmatic underplating and the lithospheric mantle. Considering this interpretation, the ~1.2 s phase on all RFs correspond to the P_cs phase, i.e. the intracrustal boundary and the ~3 s correspond to the *Pms* phase (Fig. 3D). A similar terminology was previously used by Leahy et al. (2010) at Hawaii seismic station, where magmatic underplating was observed, inducing this kind of phase on receiver functions. In the case of Mayotte Island, the development of a thick underplating despite a volcanic activity which is much less intense than in Iceland or Hawaii, may result from the 20-Myrs-long duration of the volcanism (Michon, 2016).

Lemoine et al. (2020) and Cesca et al. (2020) proposed that the current submarine eruption east of Mayotte is fed by a magma reservoir located at 28 km and 30 ± 5 km depth, respectively. Our results (*Moho* at of 26–27 km depth) may therefore suggest that this magma reservoir developed below the interface between the mantle lithosphere and the underplating. Moreover, the seismicity related to the volcano-tectonic crisis of Mayotte, which is almost exclusively located below 30 km depth (see ReVoSiMa Bulletins at http://www.ipgp.fr/fr/actualites-reseau), likely occurs below the magmatic underplated layer, i.e., into the mantle lithosphere.

Grande Glorieuse Island. Data for Grande Glorieuse reveal two seismic discontinuities at 1 and 5 km depth below the station. The first one may be related to the submarine sedimentary platform located at around 1 km below sea level (Courgeon et al., 2016). The small amplitude of the first phase is consistent with results from RF modeling, which shows the link between a small amplitude of the first peak and a thin low-velocity sedimentary layer (Zelt and Ellis, 1999). The boundary observed at 5 km may represent the interface between the volcanic edifice and the crust. The relatively large depth of this interface may be attributed to the

subsidence of the at least 60 Ma-old volcanic edifice (Courgeon et al., 2016; Leroux et al., 2020), which is supported by the step-by-step development of a carbonate platform over the volcano (Jorry et al., 2016) and absolute datation (Leroux et al., 2020). Both RF methods revealed a *Moho* discontinuity at 11 km depth. Therefore, the crustal thickness is estimated to 6 km beneath the island, which is close to the average thickness of oceanic crust (White et al., 1992). The high V_P/V_S ratio (~2.0) may be explained by both the effects of bioconstructions on the top of the edifice and the underlying mafic rocks (Christensen, 1996). In the vicinity of Grande Glorieuse, the occurrence of WSW-ENE magnetic anomalies associated with the Somali Basin (Phethean et al., 2016) fully supports an oceanic crustal nature below this island.

5.2. Implication of the continental nature of the crust below Mayotte in the opening of the Somali and Comoros basins

The occurrence of sandstone xenoliths in the lavas of the Comoros archipelago (Flower and Strong, 1969) and a km-scale massif of quartzite in the volcanic island of Anjouan (Esson et al., 1970) have long been considered as evidences of a continental crust below the Comoros archipelago. Our results (i.e. V_P/V_S ratio of 1.66 and 17-km-thick initial crust without considering the magmatic underplating) strongly support such a continental nature of the crust. Thus, both geological and now geophysical data suggest the occurrence of continental crust between the Somali and Comoros basins, likely as thinned crustal remnants. The oceanic nature of the crust below the Somali Basin is known from well-identified magnetic anomalies between M22 to M0 (Cochran, 1988; Phethean et al., 2016) and confirmed with our results for Grande Glorieuse Island. South of the Comoros archipelago, the lack of clear magnetic anomaly in the Comoros Basin has been interpreted as the result of an oceanic crust formation during the Jurassic quiet zone (Coffin and Rabinowitz, 1987). Recently, its oceanic nature has been confirmed by seismic refraction and gravity data (Vormann et al., 2020). The Comoros continental block would consequently correspond to an isolated piece of thinned continent block abandoned during the southward drift of Madagascar. Such isolated blocks have been already described in the break-up of continental lithospheres and may result from a wide range of processes such as rotational extension, changing extension directions, rift migration, thinning processes (Péron-Pinvidic and Manatschal, 2010; Naliboff and Buiter, 2015; Whittaker et al., 2016; Molnar et al., 2018). Regionally, the Seychelles archipelago stands as a regional example of this kind of continental blocks abandoned during continental break-up, in this case between Madagascar and India (e.g. Hammond et al., 2012, 2013). The Comoros archipelago lies on a crust cut by N140-150 fracture zones that are also observed along the Somali passive margin and the northern Somali Basin (Phethean et al., 2016). The isolation of the Comoros continental block could have thus occurred during the initial stage of rifting. However, the lack of any robust age constraints and geophysical data on the structure of the Comoros Basin does not help determining the mechanism that led to the isolation of this continental domain.

6. Conclusions

We measured the seismic velocity structure and the crust thickness beneath islands of the Mozambique Channel from receiver function using both Neighborhood Algorithm and H-κ stacking approaches. Despite a limited dataset due to the short duration of deployment of the seismic stations and subsequently to a relatively small number of seismic events, we were able to bring new elements on the nature(s) and thickness of the crust in this region. From RF studies, we propose that the volcanic edifice of Mayotte Island is emplaced on an isolated continental block abandoned during the dismantling of Gondwana and later thickened by magmatic underplating. Our results indicate that Grande Glorieuse Island is underlain by a normal oceanic crust, confirming the oceanic nature of the crust northeast of Mayotte. Juan de Nova Island lies over a clearly thinned continental crust, which is consistent with a prograding ocean-continent transition toward the Davie Ridge (Vormann et al., 2020). Beneath Europa Island, the best ensemble of S-wave velocity profiles suggest instead a thick oceanic crust, which would result from a magmatic underplating accumulation related to successive regional magmatic events. Beside these results on the nature of the crust below the islands of the Mozambique Channel, our S-wave velocity profiles defined down to 60 km depth beneath Mayotte should improve the relocation of the deep seismicity occurring during the ongoing 2018–2020 seismo-volcanic crisis and consequently our knowledge on the processes occurring in the deeper lithosphere. Finally, further geophysical and geochemical studies could help strengthening our interpretations based on a limited dataset.

Data availability

Datasets for this research are available on https://doi.org/10.15778/RESIF.YV2011 from the French RESIF data center (http://seismology.resif.fr, Barruol et al., 2017).

Declaration of competing interest

The authors declare that they have no known competing financial interests or personal relationships that could have appeared to influence the work reported in this paper.

Acknowledgements

A. Dofal benefited from a Ph.D. grant of the University of La Réunion. This work was supported by the Programme Iles Eparses funded by the CNRS-INSU (Institut National des Sciences de l'Univers), CNRS-INEE (Institut National Ecologie et Environnement), TAAF (Terres Australes et Antarctiques Françaises), and by the RHUM-RUM project (www.rhum-rum.net) funded by the ANR (Agence Nationale de la Recherche) in France (project ANR-11-BS56-0013), and by the DFG (Deutsche Forschungsgemeinschaft) in Germany. Additional funding has been provided by the INSU program SYSTER, the OSU-Réunion (Observatoire des Sciences de l'Univers). Portable seismometers were provided by the Alfred Wegener Institut (AWI) in Bremerhaven. We thank C. Davy, E. Delcher, A. Nercessian, C. Brunet, K. Sigloch and G. Roult for their help with installation and maintenance of the seismic stations. We are grateful to J. Vergne for his H-κ stacking code. We also thank the three anonymous reviewers who contributed to the improvement of the manuscript. This is IPGP contribution 4121.

Appendix A. Supplementary data

Supplementary data to this article can be found online at https://doi.org/10.1016/j.jafrearsci.2021.104379.

References

Andriampenomanana, F., Nyblade, A.A., Wysession, M.E., Durrheim, R.J., Tilmann, F., Julià, J., Pratt, M., Rambolamanana, G., Aleqabi, G., Shore, P., Rokotondraibe, 2017. The structure of the crust and uppermost mantle beneath Madagascar. Geophys. J. Int. 210 (3), 1525–1544. https://doi.org/10.1093/gji/ggx243.

Artemieva, I., 2011. The Lithosphere: an Interdisciplinary Approach. Cambridge University Press, p. 794.

Audru, J.-C., Guennoc, P., Thinon, I., Abellard, O., 2006. Bathymay : la structure sous-marine de Mayotte révélée par l'imagerie multifaisceaux. Compt. Rendus Geosci. 338 (16), 1240–1249. https://doi.org/10.1016/j.crte.2006.07.010.

Barruol, G., Sigloch, K., 2013. Investigating La réunion hot spot from crust to core. Eos, Transactions American Geophysical Union 94 (23), 205–207. https://doi.org/10.1002/2013EO230002.

Barruol, G., Sigloch, K., RHUM-RUM Group, RESIF, 2017. RHUM-RUM experiment, 2011-2015, code YV (réunion hotspot and upper mantle – réunion's unterer Mantel) funded by ANR, DFG, CNRS-INSU, IPEV, TAAF, instrumented by DEPAS, INSU-OBS, AWI and the universities of muenster, bonn, La réunion [data set]. RESIF - Réseau Sismologique et géodésique Français. https://doi.org/10.15778/RESIF.YV2011.

Barruol, G., Sigloch, K., Scholz, J.-R., Mazzullo, A., Stutzmann, E., Montagner, J.-P., Kiselev, S., Fontaine, F.R., Michon, L., Deplus, C., Dyment, J., 2019. Large-scale flow of Indian Ocean asthenosphere driven by Réunion plume. Nat. Geosci. 12, 1043–1049. https://doi.org/10.1038/s41561-019-0479-3.

Bassias, Y., Leclaire, L., 1990. The Davie Ridge in the Mozambique channel: crystalline basement and intraplate magmatism. Neues Jahrbuch Geol. Palaontol. Monatsh. 2, 67–90. https://doi.org/10.1127/njgpm/1990/1990/67.

Bonvalot, S., Balmino, G., Briais, A., Kuhn, M., Peyrefitte, A., Vales, N., et al., 2012. World Gravity Map. Bureau Gravimetrique International (BGI), Map, CGMW-BGI-CNES728, IRD, Paris.

Cesca, S., Letort, J., Razafindrakoto, H.N.T., Heimann, S., Rivalta, E., Isken, M.P., Nikkhoo, M., Passarelli, L., Petersen, G.M., Cotton, F., Dahm, T., 2020. Drainage of a deep magma reservoir near Mayotte inferred from seismicity and deformation. Nat. Geosci. 13 (1), 87–93. https://doi.org/10.1038/s41561-019-0505-5.

Chatterjee, S., Goswami, A., Scotese, C.R., 2013. The longest voyage: tectonic, magmatic, and paleoclimatic evolution of the Indian plate during its northward flight from Gondwana to Asia. Gondwana Res. 23 (1), 238–267. https://doi.org/10.1016/j.gr.2012.07.001.

Christensen, N.I., 1996. Poisson's ratio and crustal seismology. J. Geophys. Res.: Solid Earth 101 (B2), 3139–3156. https://doi.org/10.1029/95JB03446.

Cochran, J.R., 1988. Somali basin, chain ridge, and origin of the northern Somali basin gravity and geoid low. J. Geophys. Res. 93 (B10), 11985–12008. https://doi.org/10.1029/JB093iB10p11985.

Coffin, M.F., Rabinowitz, P.D., 1987. Reconstruction of Madagascar and Africa: evidence from the Davie fracture zone and western Somali basin. J. Geophys. Res. 92 (B9), 9385–9406. https://doi.org/10.1029/JB092iB09p09385.

Courgeon, S., Jorry, S.J., Camoin, G.F., BouDagher-Fadel, M.K., Jouet, G., Révillon, S., Bachèlery, P., Pelleter, E., Borgomano, J., Poli, E., Droxler, A.W., 2016. Growth and demise of Cenozoic isolated carbonate platforms: new insights from the Mozambique Channel seamounts (SW Indian Ocean). Mar. Geol. 380, 90–105. https://doi.org/10.1016/j.margeo.2016.07.006.

Courgeon, S., Jorry, S.J., Jouet, G., Camoin, G., BouDagher-Fadel, M.K., Bachèlery, P., Caline, B., Boichard, R., Révillon, S., Thomas, T., Thereau, E., Guérin, C., 2017. Impact of tectonic and volcanism on the Neogene evolution of isolated carbonate platforms (SW Indian Ocean). Sediment. Geol. 355, 114–131. https://doi.org/10.1016/j.sedgeo.2017.04.008.

Courgeon, S., Bachèlery, P., Jouet, G., Jorry, S.J., Bou, E., BouDagher-Fadel, M.K., Révillon, S., Camoin, G., Poli, E., 2018. The offshore east African rift system: new insights from the Sakalaves seamounts (Davie Ridge, SW Indian Ocean). Terra. Nova 15, 321–329. https://doi.org/10.1111/ter.12353.

Cox, K.G., 1992. Karoo igneous activity, and the early stages of the break-up of Gondwanaland. Geological Society, London, Special Publications 68 (1), 137–148. https://doi.org/10.1144/GSL.SP.1992.068.01.09.

Davis, J.K., Lawver, L.A., Norton, I.O., Gahagan, L.M., 2016. New Somali Basin magnetic anomalies and a plate model for the early Indian Ocean. Gondwana Res. 34, 16–28. https://doi.org/10.1016/j.gr.2016.02.010.

Deville, E., Marsset, T., Courgeon, S., Jatiault, R., Ponte, J.-P., Thereau, E., Jouet, G., Jorry, S., Droz, L., 2018. Active fault system across the oceanic lithosphere of the Mozambique Channel: implications for the Nubia–Somalia southern plate boundary. Earth Planet Sci. Lett. 502, 210–220. https://doi.org/10.1016/j.epsl.2018.08.052.

de Wit, M.J., 2003. Madagascar: heads it's a continent, tails it's an island. Annu. Rev. Earth Planet Sci. 31, 213–248. https://doi.org/10.1146/annurev.earth.31.100901.141337.

Esson, J., Flower, M.F.J., Strong, D.F., Upton, B.G.J., Wadsworth, W.J., 1970. Geology of the comores archipelago, western Indian ocean. Geol. Mag. 107 (6), 549–557. https://doi.org/10.1017/S0016756800058647.

Famin, V., Michon, L., Bourhane, A., 2020. The Comoros archipelago_ a right-lateral transform boundary between the Somalia and Lwandle plates. Tectonophysics 789, 228539. https://doi.org/10.1016/j.tecto.2020.228539.

Feuillet, N., Jorry, S., Crawford, W.C., Deplus, C., Thinon, I., Jacques, E., Saurel, J.M., Lemoine, A., Paquet, F., Satriano, C., Aiken, C., Foix, O., Kowalski, P., Laurent, A., Rinnert, E., Cathalot, C., Donval, J.-P., Guyader, V., Gaillot, A., Scalabrin, C., Moreira, M., Peltier, A., Beauducel, F., Grandin, R., Ballu, V., Daniel, R., Pelleau, P., Gomez, J., Besançon, S., Geli, L., Bernard, P., Bachelery, P., Fouquet, Y., Bertil, D., Lemarchand, A., Van der Woerd, J., 2021. Birth of a large volcanic edifice offshore Mayotte via lithosphere-scale dyke intrusion. Nat. Geosci. https://doi.org/10.1038/s41561-021-00809-x.

Flower, M.F.J., Strong, D.F., 1969. The significance of sandstone inclusions in lavas of the Comores archipelago. Earth Planet Sci. Lett. 7 (1), 47–50. https://doi.org/10.1016/0012-821X(69)90010-7.

Flower, M.F.J., 1972. Petrology of volcanic rocks from Anjouan, Comores archipelago. Bull. Volcanol. 36 (1), 238–250. https://doi.org/10.1007/BF02596993.

Fontaine, F.R., Tkalčić, H., Kennett, B.L.N., 2013a. Imaging crustal structure variation across southeastern Australia. Tectonophysics 582, 112–125. https://doi.org/10.1016/j.tecto.2012.09.031.

Fontaine, F.R., Tkalčić, H., Kennett, B.L.N., 2013b. Crustal complexity in the Lachlan Orogen revealed from teleseismic receiver functions. Aust. J. Earth Sci. 60 (3), 413–430. https://doi.org/10.1080/08120099.2013.787646.

Fontaine, F.R., Barruol, G., Tkalčić, H., Wolbern, I., Rümpker, G., Bodin, T., Haugmard, M., 2015. Crustal and uppermost mantle structure variation beneath La Réunion hotspot track. Geophys. J. Int. 203 (1), 107–126. https://doi.org/10.1093/gji/ggv279.

Franke, D., Jokat, W., Ladage, S., Stollhofen, H., Klimke, J., Lutz, R., Mahanjane, E.S., Ehrhardt, A., Schreckenberger, B., 2015. The offshore East African Rift System: structural framework at the toe of a juvenile rift. Tectonics 34 (10), 2086–2104. https://doi.org/10.1002/2015TC003922.

Gallart, J., Driad, L., Charvis, P., Sapin, M., Hirn, A., Diaz, J., de Voogd, B., Sachpazi, M., 1999. Perturbation to the lithosphere along the hotspot track of La Réunion from an offshore-onshore seismic transect. J. Geophys. Res.: Solid Earth 104 (B2), 2895–2908. https://doi.org/10.1029/98JB02840.

Georgen, J.E., Lin, J., Dick, H.J.B., 2001. Evidence from gravity anomalies for interactions of the Marion and Bouvet hotspots with the Southwest Indian Ridge: effects of transform offsets. Earth Planet Sci. Lett. 187 (3–4), 283–300. https://doi.org/10.1016/S0012-821X(01)00293-X.

Hammond, W.C., Humphreys, E.D., 2000. Upper mantle seismic wave velocity: effects of realistic partial melt geometries. J. Geophys. Res.: Solid Earth 105 (B5), 10975–10986. https://doi.org/10.1029/2000JB900041.

Hammond, J.O.S., Collier, J.S., Kendall, J.-M., Helffrich, G., Rümpker, G., 2012. Plume scar in the mantle lithosphere beneath the Seychelles revealed by seismic imaging. Earth Planet Sci. Lett. 355, 20–31. https://doi.org/10.1016/j.epsl.2012.08.020, 356.

Hammond, J.O.S., Kendall, J.-M., Collier, J.S., Rümpker, G., 2013. The extent of continental crust beneath the Seychelles. Earth Planet Sci. Lett. 381, 166–176. https://doi.org/10.1016/j.epsl.2013.08.023.

Hartnady, C., 1990. Seismicity and plate boundary evolution in southeastern Africa. S. Afr. J. Geol. 93 (3), 473–484.

Jorry, S.J., Camoin, G.F., Jouet, G., Roy, P.L., Vella, C., Courgeon, S., Prat, S., Fontanier, C., Paumard, V., Boulle, J., Caline, B., Borgomano, J., 2016. Modern sediments and Pleistocene reefs from isolated carbonate platforms (Iles Eparses, SW Indian Ocean): a preliminary study. Acta Oecol. 72, 129–143. https://doi.org/10.1016/j.actao.2015.10.014.

Klimke, J., Franke, D., Gaedicke, C., Schreckenberger, B., Schnabel, M., Stollhofen, H., Rose, J., Chaheire, M., 2016. How to identify oceanic crust—evidence for a complex break-up in the Mozambique Channel, off East Africa. Tectonophysics 693, 436–452. https://doi.org/10.1016/j.tecto.2015.10.012.

Klimke, J., Franke, D., Mahanjane, E.S., Leitchenkov, G., 2018. Tie points for Gondwana reconstructions from a structural interpretation of the Mozambique basin, East Africa and the riiser-larsen sea, Antarctica. Solid Earth 9 (1), 25–37. https://doi.org/10.5194/se-9-25-2018.

Konig, M., Jokat, W., 2010. Advanced insights into magmatism and volcanism of the Mozambique Ridge and Mozambique Basin in the view of new potential field data. Geophys. J. Int. 180 (1), 158–180. https://doi.org/10.1111/j.1365-246X.2009.04433.x.

Lamarque, G., Barruol, G., Fontaine, F.R., Bascou, J., Menot, R.-P., 2015. Crustal and mantle structure beneath the Terre Adelie Craton, East Antarctica: insights from receiver function and seismic anisotropy measurements. Geophys. J. Int. 200 (2), 807–821. https://doi.org/10.1093/gji/ggu430.

Leahy, G.M., Collins, J.A., Wolfe, C.J., Laske, G., Solomon, S.C., 2010. Underplating of the Hawaiian Swell: evidence from teleseismic receiver functions. Geophys. J. Int. 183 (1), 313–329. https://doi.org/10.1111/j.1365-246X.2010.04720.x.

Leinweber, V.T., Jokat, W., 2012. The Jurassic history of the Africa–Antarctica corridor — new constraints from magnetic data on the conjugate continental margins. Tectonophysics 530, 87–101. https://doi.org/10.1016/j.tecto.2011.11.008, 531.

Leinweber, V.T., Klingelhoefer, F., Neben, S., Reichert, C., Aslanian, D., Matias, L., Heyde, I., Schreckenberger, B., Jokat, W., 2013. The crustal structure of the Central Mozambique continental margin — wide-angle seismic, gravity and magnetic study in the Mozambique Channel, Eastern Africa. Tectonophysics 599, 170–196. https://doi.org/10.1016/j.tecto.2013.04.015.

Lemoine, A., Briole, P., Bertil, D., Roullé, A., Foumelis, M., Thinon, I., Raucoules, D., de Michele, M., Valty, P., Hoste Colomer, R., 2020. The 2018–2019 seismo-volcanic crisis east of Mayotte, Comoros islands: seismicity and ground deformation markers of an exceptional submarine eruption. Geophys. J. Int. 223 (1), 22–44. https://doi.org/10.1093/gji/ggaa273.

Leroux, E., Counts, J.W., Jorry, S.J., Jouet, G., Révillon, S., BouDagher-Fadel, M.K., Courgeon, S., Berthod, C., Ruffet, G., Bachèlery, P., Grenard-Grand, E., 2020. Evolution of the glorieuses seamount in the SW Indian ocean and surrounding deep Somali basin since the cretaceous. Mar. Geol. 427, 106202. https://doi.org/10.1016/j.margeo.2020.106202.

Ligorria, J.P., Ammon, C.J., 1999. Iterative deconvolution and receiver-function estimation. Bull. Seismol. Soc. Am. 89 (5), 1395–1400.

Lort, J.M., Limond, W.Q., Segoufin, J., Patriat, Ph, Delteil, J.R., Damotte, B., 1979. New seismic data in the Mozambique Channel. Mar. Geophys. Res. 4 (1), 71–89. https://doi.org/10.1007/BF00286146.

Mascle, J., Mougenot, D., Blarez, E., Marinho, M., Virlogeux, P., 1987. African transform continental margins: examples from Guinea, the ivory coast and Mozambique. Geol. J. 22 (S2), 537–561. https://doi.org/10.1002/gj.3350220632.

Mazzullo, A., Stutzmann, E., Montagner, J.-P., Kiselev, S., Maurya, S., Barruol, G., Sigloch, K., 2017. Anisotropic tomography around la Réunion island from Rayleigh waves: tomography of western Indian Ocean. J. Geophys. Res.: Solid Earth 122 (11), 9132–9148. https://doi.org/10.1002/2017JB014354.

Michon, L., 2016. The volcanism of the Comoros archipelago integrated at a regional scale. In: Bachelery, P., Lenat, J.-F., Di Muro, A., Michon, L. (Eds.), Active Volcanoes of the Southwest Indian Ocean. Springer Berlin Heidelberg, Berlin, Heidelberg, pp. 333–344. https://doi.org/10.1007/978-3-642-31395-0_21.

Molnar, N.E., Cruden, A.R., Betts, P.G., 2018. Unzipping continents and the birth of microcontinents. Geology 46, 451–454. https://doi.org/10.1130/G40021.1.

Mueller, C.O., Jokat, W., 2017. Geophysical evidence for the crustal variation and distribution of magmatism along the central coast of Mozambique. Tectonophysics 712–713, 684–703. https://doi.org/10.1016/j.tecto.2017.06.007.

Naliboff, J., Buiter, S.J.H., 2015. Rift reactivation and migration during multiphase extension. Earth Planet Sci. Lett. 421, 58–67. https://doi:10.1016/j.epsl.2015.03.050.

O'Connor, J.M., Jokat, W., Regelous, M., Kuiper, K.F., Miggins, D.P., Koppers, A.A.P., 2019. Superplume mantle tracked isotopically the length of Africa from the Indian ocean to the red sea. Nat. Commun. 10, 1–13. https://doi.org/10.1038/s41467-019-13181-7.

Péron-Pinvidic, G., Manatschal, G., 2010. From microcontinents to extensional allochthons: witnesses of how continents rift and break apart? Petrol. Geosci. 16, 189–197. https://doi.org/10.1144/1354-079309-903.

Phethean, J.J.J., Kalnins, L.M., van Hunen, J., Biffi, P.G., Davies, R.J., McCaffrey, K.J.W., 2016. Madagascar's escape from Africa: a high-resolution plate reconstruction for the Western Somali Basin and implications for supercontinent dispersal. G-cubed 17 (12), 5036–5055. https://doi.org/10.1002/2016GC006624.

Rabinowitz, P.D., Coffin, M.F., Falvey, D., 1983. The separation of Madagascar and Africa. Science 220 (4592), 67–69. https://doi.org/10.1126/science.220.4592.67.

Raharjo, W., Palupi, I.R., Nurdian, S.W., Giamboro, W.S., Soesilo, J., 2016. Poisson's ratio analysis (Vp/Vs) on volcanoes and geothermal potential areas in Central Java using tomography travel time method of grid search relocation hypocenter. J. Phys. Conf. 776, 012114 https://doi.org/10.1088/1742-6596/776/1/012114.

Rindraharisaona, E.J., Tilmann, F., Yuan, X., Rümpker, G., Giese, J., Rambolamanana, G., Barruol, G., 2017. Crustal structure of southern Madagascar from receiver functions and ambient noise correlation: implications for crustal evolution: crustal structure of southern Madagascar. J. Geophys. Res.: Solid Earth 122 (2), 1179–1197. https://doi.org/10.1002/2016JB013565.

Roach, P., Milsom, J., Toland, C., Matchette-Downes, C., Budden, C., Riaroh, D., Houmadi, N., 2017. New evidence supports presence of continental crust beneath the Comoros: Pesgb. Hgs Africa Conference.

Rogers, R.R., Hartman, J.H., Krause, D.W., 2000. Stratigraphic analysis of upper Cretaceous rocks in the Mahajanga basin, northwestern Madagascar: implications for ancient and modern faunas. J. Geol. 108 (3), 275–301. https://doi.org/10.1086/314403.

Sambridge, M., 1999. Geophysical inversion with a neighbourhood algorithm-I. Searching a parameter space. Geophys. J. Int. 138 (2), 479–494. https://doi.org/10.1046/j.1365-246X.1999.00876.x.

Saurel, J.-M., Aiken, C., Jacques, E., Lemoine, A., Crawford, W., Lemarchand, A., Daniel, R., Pelleau, P., Bès-de Berc, M., Dectot, G., Bertil, D., Roullé, A., Broucke, C., Colombain, A., Besançon, S., Guyavarch, P., Kowalski, P., Roudaut, M., Dofal, A., Foix, O., Géli, L., Gomez, J., Grunberg, M., Angèle, L., Léger, F., Satriano, C., Tronel, F., Van der Woerd, J., Jorry, S., Thinon, I., Feuillet, N., 2019. V43I-0220 - high-resolution onboard manual locations of Mayotte seismicity since March 2019, using local land and seafloor stations. In: Proceedings of the AGU Fall Meeting 2019. AGU.

Saurel, J.-M., Jacques, E., Aiken, C., Lemoine, A., Retailleau, L., Lavayssière, A., Foix, O., Dofal, A., Laurent, A., Mercury, N., Crawford, W., Lemarchand, A., Daniel, R., Pelleau, P., Bès de Berc, M., Dectot, G., Bertill, D., Roullé, A., Broucke, C., Coombain, A., Jund, H., Besançon, S., Guyavarch, P., Kowaski, P., Roudaut, M., Aprioual, R., Battaglia, J., Bodihar, S., Boissier, P., Bouin, M-P., Brunet, C., Canjamale, K., Catherine, P., Desfete, N., Doubre, C., Dretzen, R., Dumouche, T., Fernagu, P., Ferrazzini, V., Fontaine, F., Gaillot, A., Géli, L., Griot, C., Grunberg, M., Can Guzel, E., Hoste-Colomer, R., Lambotte, S., Lauret, F., Léger, F., Maros, E., Peltier, A., Vergne, J., Satriano, C., Tronel, F., Van der Woerd, J., Fouquet, Y., Jorry, S., Rinnert, E., Thinon, I. & Feuillet, N., Under Review to Geophysical Journal International. Mayotte Seismic Crisis: Building Knowledge in Near Real-Time by Combining Land and Ocean-Bottom Seismometers, (first results).

Scholz, J.-R., Barruol, G., Fontaine, F.R., Mazzullo, A., Montagner, J.P., Stutzman, E., Michon, L., Sigloch, K., 2018. SKS splitting in the Western Indian Ocean from land and seafloor seismometers: plume, Plate and Ridge signatures. Earth Planet Sci. Lett. 498, 169–184. https://doi.org/10.1016/j.epsl.2018.06.033.

Ségoufin, J., Patriat, P., 1981. Reconstructions de l'océan Indien Occidental pour les époques des anomalies M21, M2 et 34. Paléoposition de Madagascar. Bull. Soc. Geol. Fr. 7 (6), 600–607. https://doi.org/10.2113/gssgfbull.S7-XXIII.6.603.

Ségoufin, J., Munschy, M., Bouysse, P., Mendel, G., Grikurov, G., Leitchenkov, G., et al., 2004. Map of the Indian Ocean (1: 20,000,000), Sheet 2, Structural Map. CGMW Edition, Paris.

Senkans, A., Leroy, S., d'Acremont, E., Castilla, R., Despinois, F., 2019. Polyphase rifting and break-up of the central Mozambique margin. Mar. Petrol. Geol. 100, 412–433. https://doi.org/10.1016/j.marpetgeo.2018.10.035.

Shibutani, T., Sambridge, M., Kennett, B., 1996. Genetic algorithm inversion for receiver functions with application to crust and uppermost mantle structure beneath eastern Australia. Geophys. Res. Lett. 23 (14), 1829–1832. https://doi.org/10.1029/96GL01671.

Smith, W.H.F., Sandwell, D.T., 1997. Global seafloor topography from satellite altimetry and ship depth soundings. Science 277 (5334), 1956–1962. https://doi.org/10.1126/science.277.5334.1956.

Stamps, D.S., Calais, E., Saria, E., Hartnady, C., Nocquet, J.-M., Ebinger, C.J., Fernandes, R.M., 2008. A kinematic model for the east African Rift. Geophys. Res. Lett. 35 (5) https://doi.org/10.1029/2007GL032781.

Storey, M., Mahoney, J.J., Saunders, A.D., Duncan, R.A., Kelley, S.P., Coffin, M.F., 1995. Timing of hot spot–related volcanism and the breakup of Madagascar and India. Science 267 (5199), 852–855. https://doi.org/10.1126/science.267.5199.852.

Talwani, M., 1962. Gravity measuremants on HMS acheron in south Atlantic and Indian oceans. Geol. Soc. Am. Bull. 73 (9), 1171–1182. https://doi.org/10.1130/0016-7606(1962)73[1171:GMOHAI]2.0.CO, 2.

Tucker, R.D., Roig, J.Y., Moine, B., Delor, C., Peters, S.G., 2014. A geological synthesis of the Precambrian shield in Madagascar. J. Afr. Earth Sci. 94, 9–30. https://doi.org/10.1016/j.jafrearsci.2014.02.001.

Vormann, M., Franke, D., Jokat, W., 2020. The crustal structure of the southern Davie Ridge offshore northern Mozambique – a wide-angle seismic and potential field study. Tectonophysics 778, 228370. https://doi.org/10.1016/j.tecto.2020.228370.

Wadati, K., others, 1933. On the travel time of earthquake waves. Geophys. Mag., Tokyo 7 (87–15 3), 187–194, 269–90; 8.

White, R.S., McKenzie, D., O'Nions, R.K., 1992. Oceanic crustal thickness from seismic measurements and rare earth element inversions. J. Geophys. Res. 97 (B13), 19683–19715. https://doi.org/10.1029/92JB01749.

Whittaker, J.M., Williams, S.E., Halpin, J.A., Wild, T.J., Stilwell, J.D., Jourdan, F., Daczko, N.R., 2016. Eastern Indian Ocean microcontinent formation driven by plate motion changes. Earth Planet Sci. Lett. 454, 203–212. https://doi.org/10.1016/j.epsl.2016.09.019.

Zelt, B.C., Ellis, R.M., 1999. Receiver-function studies in the trans-hudson orogen, saskatchewan, *Canadian Journal of*. Earth Sci. 36 (4), 585–603. https://doi.org/10.1139/e98-109.

Zhang, T., Lin, J., Gao, J., 2011. Interactions between hotspots and the Southwest Indian Ridge during the last 90 Ma: implications on the formation of oceanic plateaus and intra-plate seamounts. Sci. China Earth Sci. 54 (8), 1177–1188. https://doi.org/10.1007/s11430-011-4219-9.

Zheng, Y., Lay, T., 2006. Low V_P/V_S ratios in the crust and upper mantle beneath the Sea of Okhotsk inferred from teleseismic p_MP, s_MP, and s_MS underside reflections from the Moho. J. Geophys. Res. 111 (B1) https://doi.org/10.1029/2005JB003724.

Zhu, L., Kanamori, H., 2000. Moho depth variation in southern California from teleseismic receiver functions. J. Geophys. Res.: Solid Earth 105 (B2), 2969–2980. https://doi.org/10.1029/1999JB900322.